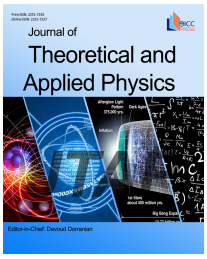

Volume 19, Issue 2, 192521 (1-15)

Journal of Theoretical and Applied Physics (JTAP)

https://doi.org/10.57647/j.jtap.2025.1902.21

Role of the atomic argon on the plasma characteristics of O_2/N_2 gas mixture

Saeed Karimian[1], Sanaz Payandeh[2], Zahra Emam Bakhsh[3], Amir Falahat[3], Ali Barkhordari[2,*]

[1]*Department of Physics, Vali-e-Asr University of Rafsanjan, Rafsanjan, Iran.*
[2]*Faculty of Physics, Shahid Bahonar University of Kerman, Kerman, Iran.*
[3]*Photonics Research Institute, Graduate University of Advanced Technology, Kerman, Iran.*

[*]**Corresponding author:** alibarkhordari20gmail.com

Original Research

Received:
28 January 2025
Revised:
25 March 2025
Accepted:
3 April 2025
Published online:
10 April 2025

Abstract:

The current work conducts a detailed investigation on adding atomic argon to the O_2/N_2 plasma in direct current (DC) and radiofrequency (RF) atmospheric plasma jets (APJs) using Optical Emission Spectroscopy (OES). The plasma density, rotational, vibrational, and excitation temperatures are determined by studying emission spectra obtained near the DC and RF APJs plume. The NO and OH bands are seen in the emission spectrum. The three N_2 vibrational bands and the Ar I spectral emission line intensities are used to calculate the vibrational and excitation temperatures. The emission intensity from argon ions increases with larger argon contributions in the $Ar/O_2/N_2$ gaseous mixture in both APJs. Furthermore, when the argon contribution to the mixture is high and nitrogen is greater than oxygen, the plasma electron density decreases as the rotational, vibrational, and excitation temperatures rise. However, for both the generated APJs, when oxygen contributes more than nitrogen and increases plasma electron density, the vibrational and rotational temperatures fall. However, larger input DC and RF powers result in higher plasma density and rotational, vibrational, and excitation temperatures for both DC and RF APJs. Furthermore, the molecular oxygen and nitrogen dissociation rate increases as the amount of argon in the mixture increases.

Keywords: DC and RF APJs; $Ar/O_2/N_2$ gas mixture; Optical emission spectroscopy (OES); Actinometry

1. Introduction

Due to the sufficiently low temperatures of various generated species in the cold atmospheric plasma discharge media under operating conditions, these devices are recognized as reliable and intriguing tools for plasma sterilization and disinfection procedures. Compared to the chemical compounds now utilized in chemical treatments, they pose lower threats to human health and the environment. Furthermore, cold plasma discharges are appropriate for large-scale sterilization and disinfection procedures because they can deactivate and eradicate biological pathogens like bacterial spores and endotoxins [1–11], various polypeptides [12–17], and yeasts [3]. Furthermore, much technological work and research has been done recently on the different manufactured APJs. Nonetheless, the long-lived reactive species that are generated could be important for the many technological uses of APJs. As a result, numerous devices with varied electrode configurations, power sources, and gaseous mixtures have been created thus far in order to have the plasma discharge under varied operating conditions [6–18]. Because $Ar/O_2/N_2$ plasma discharges emit UV light, the effectiveness of eliminating biomolecules using them can be greatly enhanced [19]. This is especially true when the amount of argon in the combination is larger. Additionally, the produced excited species in the $Ar/O_2/N_2$ plasma discharge will emit photons from the molecules and excited atoms like NO and Ar^* at wavelengths that are below 275 nm, or in the VUV/UV range. The energy of these photons is sufficient to cause significant breaks in the DNA structure [20]. They are also appropriate for breaking the bonds in solid materials. Noteworthy are the synergistic effects of several species and radiation emissions in the plasma discharge medium of APJs [18–23].

Stapelmann et al. [18] investigated the technical and physical characteristics of the ICP plasma discharges with the different $Ar/N_2/O_2$ gaseous mixtures using the OES method. Evaluating the circumstances resulting in the high UV radi-

ation intensity was the primary goal. It was demonstrated that a gaseous discharge containing an $Ar/O_2/N_2$ mixture was more appropriate for sterilizing and decontaminating surfaces than discharges containing both Ar/O_2 and O_2/N_2 gaseous mixtures. Nonetheless, the most widely utilized binary combinations for harmful biomolecule removal and microorganism inactivation. Furthermore, when compared to plasma discharge using the Ar/O_2 and O_2/N_2 gaseous mixture, the wavelength of UV created in the formed plasma is far more effective in inactivating bacterial spores.

Kutasi et al. [24] determined the effects of various parameters of an afterglow plasma discharge system. Their research focused on the effects of surface wave discharges on the composition of the afterglow plasma in the gaseous combination of $Ar/O_2/N_2$. Through studies using mass spectrometry, their kinetic model was verified. In addition, different pressures were applied to the discharge area. They compared the generated plasma discharges in the binary and ternary gaseous mixtures at a gas pressure of 8 mbar. It was determined that in both binary and ternary gaseous mixtures, the N_2/O_2 gas ratio has a substantial impact on the density of the generated plasma discharge. The amount of atomic nitrogen in both mixtures is nearly equal for very low N_2/O_2 gas ratios. However, the atomic nitrogen number density in these combinations will differ by an order of magnitude at the higher ratios. Furthermore, the UV radiations in the binary and ternary gaseous mixtures were equivalent at the same oxygen content.

Greenfield et al. [25] developed a DC APJ with a helical configuration to track the route of charged particles between two metallic electrodes. As a result, the application of a low-voltage DC with an electrical current between 20 and 40 A resulted in the production of the plasma discharge. This plasma's kinetic energy of various generated species makes it appropriate for spectroscopic applications. Furthermore, it was discovered that solid particulate matter analysis could be performed using the emission from the DC plasma. It's interesting to note that it can analyze materials that are liquid or solid. In addition, this DC plasma jet is less flexible as a lab instrument than other plasma sources like RF power generators. To use a glass chip for spectro-chemical analysis, Bessoth et al. [26] investigated the properties of an atmospheric pressure DC micro-plasma source with applied voltage and current of 500 V and 250 μA. The many technical aspects of the DC APJ were investigated through the use of an emission spectroscopy approach, while two tungsten electrodes were utilized to produce plasma discharge. It was discovered that as greater powers were applied to the electrodes, the emission intensity from the plasma discharge medium increased. Furthermore, it was demonstrated that the position within the micro-plasma column affects the emission of atoms and molecules.

Wilson et al. [27] created an atmospheric pressure glow micro-plasma between the two liquids that are kept in the micro-reservoirs that are grown on a glass substrate. Their technique worked by allowing liquid to sputter into the discharge medium from the cathode electrode. The amounts of Na, Pb, Al, and Cr were found to be less than 10 ppm when a commercial spectrometer was employed. It was also demonstrated that the matching spectrum intensity for the Na/N_2 ratio was suitable for assessing the concentration of Na impurities. Franzke et al. [28] created a DC plasma discharge device for use in spectrochemical analysis. Their DC plasma discharge source might function at atmospheric pressures even at low pressures. The appropriateness of the RF power source for their DBD system was demonstrated, taking into account the constraints on the spectrum measurements. It was demonstrated that greater exchange rates are utilized by plasma discharges with a high mean power density. For spectrochemical investigation, Andrade et al. [29] created a flexible DC light discharge using helium gas at atmospheric pressures in a pin-to-plate configuration. The measured current-voltage behavior and spectroscopic properties showed that the produced plasma discharge is in the glow domain, even though it was operating at high pressures. It was discovered that the discharge functions in its stable form when the applied voltage is normally between 300 and 900 V and the applied current is between 10 and 100 mA. Furthermore, rotational temperature profiles in the $1300-1600$ K region were obtained utilizing the OH emission spectra.

In prior research, the excited Ar/N_2 optical emission spectra in the plasma discharge medium of a generated atmospheric pressure pulsed DBD APJ were examined [30]. There was a range of 75 to 95% Ar contribution in the Ar/N_2 combination. At 95% Ar presence in the mixture, there was an increased emission intensity from the discharge medium. Furthermore, it was noted that the emission line intensities increased nonlinearly with increasing argon percentages in the mixture. Furthermore, plasma temperatures and densities rise and fall in proportion to the increasing argon contributions in the combination. The physical characteristics of a produced DC APJ using a gaseous combination of Ar and O_2 were investigated in a different study [31]. It was demonstrated that the emission intensities from argon ions rise with increasing argon contributions in the Ar/O_2 gaseous combination. Furthermore, with greater input DC currents, the vibrational and excitation temperatures rise; yet, for higher Ar percentages in the Ar/O_2 gaseous mixture, they fall. Barkhordari et al. investigated the technical features of the plasma discharge in a created DC APJ with Ar/N_2 and O_2/N_2 mixes using the OES approach. The analysis of the emission spectra yielded the rotational, vibrational, excitation, and plasma density temperatures [32]. It is demonstrated that the emission intensities of Ar^+ and oxygen atoms are greater at the higher Ar and N_2 percentages in both the Ar/N_2 and O_2/N_2 gaseous mixtures. Furthermore, the rotational, vibrational, and excitation temperatures rise with increasing Ar and O_2 contributions in both gaseous mixes. Furthermore, with an O_2/N_2 gaseous combination, the plasma electron density falls, but for Ar/N_2, it increases. In addition, the excitation temperature and electron density of the intended RF APJ are determined by analyzing the optical emission spectra obtained from the excited atomic Ar/O_2 in the plasma discharge in the RF APJ [33]. It was discovered that the emission intensities from atomic oxygen are greater at the larger Ar contributions in the combination. Additionally, there is a linear rise in the line intensities

from argon atoms and ions, which include oxygen atoms. Moreover, the electron density increased with increasing Ar percentages in the Ar/O_2 combination while the excitation temperature dropped. In addition, the argon excitation and nitrogen vibrational temperatures were computed using the acquired optical emission spectra from the excited Ar/N_2 in a tailored RF APJ [34]. It was observed that the emission intensity from all generated species in the plasma discharge medium of the RF APJ rises with an increase in the amount of argon in the mixture. Furthermore, both the nitrogen vibrational temperature and the argon excitation temperature rose at reduced Ar contributions in the combination.
Samarasekara et al. [35] demonstrated, using an RF plasma sputtering apparatus, that all of the thin films are sputtered on the polycrystalline Al_2O_3 substrates from the custom-made Li mixed ferrite bar targets, which have dimensions of 1 cm by 1 cm by 4 cm. At the substrate temperature, the generated thin films were deposited on the substrate. Additionally, the temperature inside the plasma column of a capillary discharge-which served as a spectroscopic light source-was determined by Lee et al. [36]. It was discovered that the plasma took only a microsecond to attain a Local Thermodynamic Equilibrium (LTE) state. They put up an empirical relationship between capillary radius and temperature.
In the current study, the plasma electron density, excitation, rotational, and vibrational temperatures of both the produced DC and RF APJs operating with $Ar/O_2/N_2$ gaseous mixture are estimated to study the effect of adding atomic argon to the O_2/N_2 plasma. It is performed by employing the OES technique and analysis of the resulting spectra emission. In order to do this, the effects of changes in the electrical power and the atomic argon gas contribution on the two APJs are investigated. Moreover, the performance of these APJs is examined in relation to the formation of argon metastable species in the discharge medium. It should be mentioned that the production of the oxygen and nitrogen species in the fabricated DC and RF APJs is examined by the actinometry method.

2. Method and devices

This research examines the effects of varying the argon contribution and input electrical powers on the O_2/N_2 plasma in the DC and RF APJs. It is vital to remember that the frequency of the power source used for plasma formation matters because it affects how the electrons, ions, and uncharged species behave in the created plasma discharge medium. Lower frequencies cause the electrons and ions to follow the electric field and be affected by its oscillations. In contrast, the plasma electrons will only react to the electric field when the power source runs at the radio frequencies. Nonetheless, the average electric field causes the plasma discharge ions to react. Miniaturized APJs are also becoming more and more common in technical applications of APJs for particular biological uses. DC APJs often have cheap operating costs and are portable. Although both of the created APJs theoretically satisfy these requirements, the DC APJ is less sophisticated than the RF APJ. Additionally, the RF APJ may operate from a high or low-power source. It affects the plasma's characteristics, demonstrating its potential for use in bio-decontamination and medicine [37]. On the other hand, the kind of plasma source and the physical and technical properties of the produced plasma discharge in the APJ plume have the greatest impact on the plasma sterilizing factors [38]. Furthermore, biopolymer treatment and tissue engineering can benefit greatly from the use of both RF and DC APJs. However, the plasma discharge in both the RF and DC APJs is non-thermal because the treatment regions need to be kept free of products that result from electrode erosion. As a result, they may be incredibly useful instruments in a range of medical settings. Interestingly, the creation of various contaminants in the plasma discharge medium is prevented in RF APJs because there is no direct contact between the plasma and electrodes [39].
In this research, the input power ranges from 0 to 50 W in the RF APJ, whereas in the DC APJ, the applied voltage and electrical current change from 0 to 7 kV and 0 to 50 mA, respectively. Furthermore, the frequency of the created RF APJ was set at 13.56 MHz. The gaseous combination of $Ar/O_2/N_2$ entered the jet tube forms the plasma plumes in both APJs [32–34]. Furthermore, the optical fiber probe was positioned 5 mm from the plasma jets' nozzle, which was 10 mm spatially apart and perpendicular to the jets' plume. It must be noted that the output RF power and impedance were first adjusted to find the best stable APJ for each argon and oxygen mixture. A lumped L-type network was utilized in the impedance-matching network operated on a transmission line. It should be mentioned that the L-type matching network was lossless, or that, with the right component selections, the loss may be made very modest. Nonetheless, the application and the RF APJs size determine the RF input power.
Here, two spectrometers are employed for the spectroscopic characterization of the plasma discharge. The HR4000 Ocean Optic and Jobin Yvon, TRIAX550 spectrometers were applied for spectroscopic measurements and calculation of the plasma parameters. It should be mentioned that a light source that can produce the spectrum emission lines has to be supplied to calibrate these spectrometers. whereby a Mercury-Argon HG-1 lamp was employed. Furthermore, using a gas mixer, the atomic argon gas-which serves as the primary carrier gas-was combined in varying proportions with the molecular oxygen and nitrogen gases. It is important to highlight that the plasma plume in both generated plasma jets seems homogenous and can extend beyond 20 mm in length.
Furthermore, the external circuit's operating parameters were set for both the produced DC and RF APJs. With the Ar, O_2, and N_2 flow rates of (1) 1.5, 0.1-1, and 0.4 SLM (Standard Liters per Minute) and (2) 1.5, 0.4, and 0.1-1 SLM, respectively, the $Ar/O_2/N_2$ gaseous mixture was entered the DC and RF APJs via the gas mixer. It is important to note that a velocity gas flow controller was used to regulate these flow rates. Here, the parameters of the DC and RF APJs were investigated under the following three operating conditions: (1) $Ar/O_2/N_2$ ratio was fixed at 6:1:3, applied DC and RF powers ranged from 10 to 50 W, (2) $Ar/O_2/N_2$

ratio was varied from 8:1:1 to 5:4:1, and (3) $Ar/O_2/N_2$ ratio was varied from 8:1:1 to 5:1:4, while applied DC and RF energies were fixed at 50 W.

The generated DC and RF APJs with the $Ar/O_2/N_2$ gaseous combination both functions according to the corona discharge mechanism, which is important to mention. In general, their plasma discharge media exhibit a much greater ionization rate than other plasma jets due to their unique geometric structures and non-uniform electric field [40–42]. Furthermore, the below arcing onset tiny discharge powers are carried by the DC and RF corona discharges. Consequently, the discharge medium of these APJs does not produce any electrical shock [43]. Furthermore, these APJs are capable of ionizing these gaseous mixtures and generating a plasma plume with a range of controlled and operational characteristics. Furthermore, in comparison to previously established APJs that operate with alternative power sources including AC and microwave power sources, these DC and RF APJs may produce plasma discharges at lower temperatures [17, 18, 29, 44]. Hensel et al. [45, 46], for instance, determined that the microwave and AC APJs rotational temperatures ranged from 750 to 4700 K. Additionally, Kutasi et al. [24] determined that the microwave plasma jet's rotational temperature was 700 K. As a result, both of them are appropriate for use in medical settings, particularly in skin treatment procedures [19]. In addition, the primary carrier gas, argon, is responsible for both the formation of reactive species and the production of a steady, uniform plasma discharge. Consequently, there is no glow-to-arc transition at all.

3. Results and discussions

Electron collision processes often excite many plasma species to higher states in plasma discharge media, where they decay and release photons with distinct wavelengths. These photons may be identified and examined by taking a record of the plasma discharge medium's emission spectrum. In this work, the various generated reactive species in $Ar/O_2/N_2$ APJs are identified using the OES approach. Their operating parameters are computed as a result. The emission spectra of the DC and RF APJs with a 6:1:3 ratio of $Ar/O_2/N_2$ gaseous mixture are displayed in figure 1. Note that the findings shown here are for 50 W DC and RF input powers at atmospheric pressure and in the $200-1000$ nm spectral wavelength range.

Figure 1 illustrates that the UV area, which falls between 210 and 300 nm in wavelength, is the primary feature of the radiated spectra. It is possible to observe the NO emission lines from the NOγ ($A^2\Sigma^+ \rightarrow X^2\Pi_r$) electronic transitions. The dissociation of oxygen and nitrogen molecules in the plasma discharge medium of DC and RF APJs, or the electron collision process, are the two processes that produce NO radicals [42]. The following is how the discovered NOγ band emerged from the collisions with the N_2 metastable state [47, 48]:

Excitation: $N_2\ (A^3\Sigma_u^+) + NO\ (X^2\Pi) \rightarrow N_2\ (X^2\Sigma_g) + NO\ (A^2\Sigma^+)$

Radiative transition: $NO\ (A^2\Sigma^+) \rightarrow NO\ (X^2\Pi) + h\nu$ (NO$-\gamma$ band)

Moreover, the OH emission bands ($A^2\Sigma,\ v = 0 \rightarrow X^2\Pi,\ v' = 0$) are seen at a wavelength of 309 nm. It is important to remember that the dissociation of water vapors in the ambient air around them is what leads to the creation of OH radicals [49]. For instance, there are three possible methods to create the excited state OH:

(1) By the direct impact between the electron and water, $H_2O + e^- \rightarrow OH\ (A^2\Sigma) + H + e^-$

(2) via H_2O^+ dissociative recombination, where H_2O^+ is formed by the metastable species of atomic argon and the subsequent dissociative recombination process [47]

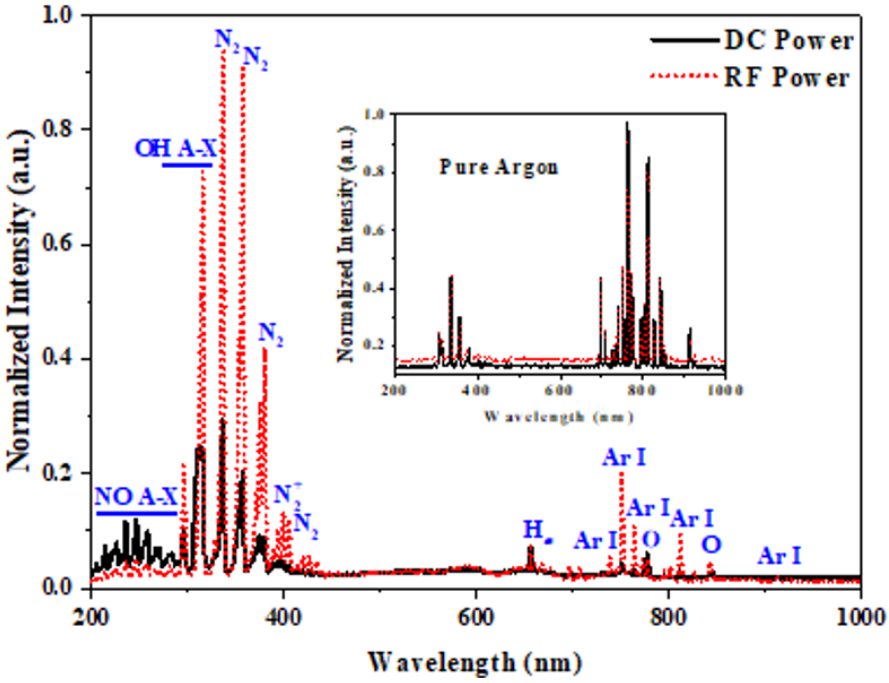

Figure 1. The recorded emission spectra of the DC and RF APJs with $Ar/O_2/N_2$ (6:1:3) at the applied power of 50 W.

$H_2O^+ + e^- \rightarrow OH\ (A^2\Sigma) + H$
and, (3) by the direct collision between the excited argon atoms and the neutral H_2O molecules as [50]:
$Ar^* + H_2O \rightarrow OH\ (A^2\Sigma) + Ar + H$
The presence of the Second Positive System N_2 ($C^3\Pi_u \rightarrow B^3\Pi_g$), the First Positive System N_2 ($B^3\Pi_g \rightarrow A^3\Sigma_u^+$), and the First Negative System N_2^+ ($B^2\Sigma_u^+ \rightarrow X^2\Sigma_g^+$) dominates the emission spectra from 300 to 450 nm, as shown in figure 1. These systems are the result of numerous exciting processes, including electron impact excitation from the molecular ground state N_2 ($X^1\Sigma_g^+$) and the first metastable state N_2 ($A^3\Sigma_u^+$), pooling reaction, and energy transition between the partners by collisions [48, 51]. These long-lived metastable species (with energies below 6 eV) are significant because they serve as energy reservoirs in the chemical processes occurring in the plasma. Furthermore, in flue gas cleaning applications, they create the condensed products [52].
The energy of the Ar_m^* ($^3P_2$,$^3P_0$) metastable states, 11.55 and 11.72 eV, is greater than the nitrogen molecule's threshold excitation energy (11.1 eV), where the metastable species is denoted by the subscript "m". As a result, adding argon gas to the nitrogen plasma discharge should result in a notable increase in emission line intensities and its subsequent impacts on the concentration of the nitrogen active species. The Penning effect provides the foundation for raising the active species density which could be described as [48]:
$N_2\ (X^1\Sigma_g^+) + Ar_m^*\ (^3P_2,^3P_0) \rightarrow N_2\ (C^3\Pi_u) + Ar\ (E > 11$ eV from $N_2\ (X, v = 0))$
With the characteristic of the Second Positive System's $(0-0)$ band at 336.1 nm in wavelength, the next radiative states decay and release photons as follows:
$N_2\ (C^3\Pi_u, v' = 0) \rightarrow N_2\ (B^3\Pi_g, v'' = 0) + h\nu$
Consequently, the Second Positive System's emission intensity in the (0–0) band is directly related to the N_2 ($C^3\Pi_u$) state's population density [50, 53]. The following procedure may be used to directly stimulate electron collisions from the ground state of the N_2 ($X^1\Sigma_g^+$) molecule to populate the N_2^+ ($B^2\Sigma_u^+$) excited state [49, 51]:
$N_2\ (X^1\Sigma_g^+) + e \rightarrow N_2^+\ (B^2\Sigma_u^+) + 2\ e\ (E > 18.5$ eV from $N_2(X, v = 0))$ or sequentially, which is achieved by ionizing the N_2 molecule by electron impact and, as a result, excitation of the molecular ion via subsequent electron collision as stated as follows:
$N_2\ (X^1\Sigma_g^+) + e \rightarrow N_2^+\ (X^2\Sigma_g^+) + 2\ e\ (E > 15.6$ eV from $N_2\ (X, v = 0))$
$N_2^+\ (X^2\Sigma_g^+) + e \rightarrow N_2^+\ (B^2\Sigma_u^+) + e\ (E > 3.3$ eV from N_2^+ $(X, v = 0)$ at 15.6 eV).
Moreover, based on the Penning ionization process, the ground state molecular ions can be generated by colliding the argon atoms at metastable states as follows [35]:
$N_2\ (X^1\Sigma_g^+) + Ar_m^*(^3P_2,^3P_0) \rightarrow N_2^+\ (X^2\Sigma_g^+) + Ar + e$
The effect of metastable argon atoms or electron collisions can further excite the N_2^+ ($X^2\Sigma_g^+$) state to the N_2^+ ($B^2\Sigma_u^+$) radiative state. As a result, the following radiative decays of the N_2^+ ($B^2\Sigma_u^+$) the excited state will release the distinctive photons of the First Negative System's (0–0) band at 391.4 nm in wavelength:
$N_2^+\ (B^2\Sigma_u^+, v' = 0) \rightarrow N_2^+\ (X^2\Sigma_g^+, v = 0) + h\nu$
where the $(0-0)$ band emission line intensity of the First Negative System is for the N_2^+ ($B^2\Sigma_u^+$) state population [54–56].
As figure 1 illustrates, there are emission bands of O_2^+ ($B^4\Sigma_g^- \rightarrow A^4\Pi_u$) in the $550-600$ nm wavelength range and atomic oxygen at 844.6 nm and 777.4 nm wavelengths associated with the ($3p^3P \rightarrow 3s^3S$) and ($3p^5P \rightarrow 3s^5S$) transitions, respectively. There was no sign of the powerful radiation emission from O_2. The following are important consequences of dissociative excitation processes based on electron and metastable argon influences on the emission intensity of the stimulated oxygen atoms and molecules [57]:
$e^- + O_2 \rightarrow O_2^+ + 2\ e^-$
$Ar^* + O_2 \rightarrow Ar + 2\ O$
The intensity of the emission lines from oxygen atoms to oxygen molecules will increase due to the quenching process, which occurs between metastable argon atoms and oxygen molecules.
Noteworthy, several characteristics need to be known to describe the electron lifetimes in different processes, such as metastable, resonant, permitted, and forbidden stimulated energy [58]. Furthermore, the following one-step and two-step procedures can both produce the Ar^{+*} excited state [59]: $Ar + e\ (E > 35$ eV$) \rightarrow Ar^{+*}$
$Ar^+ + e\ (E > 19.5$ eV$) \rightarrow Ar^{+*}$
Nevertheless, only a small number of electrons (above 35 eV) has sufficient energy to initiate both ionization and excitation processes simultaneously at low-temperature plasma discharges (where electron temperatures are below 4 eV). As a result, the two-step processes play a significant role in ground-state ion excitation. The required information on the ion density at the ground state, or Ar^+, is generated by this technique [60]. Furthermore, strong intensity peaks corresponding to wavelengths of 737.3 nm, 750.4 nm, 763.5 nm, and 811.7 nm are identified for the argon plasma discharge associated with Ar I 4*s*–4*p*, 4*p*–6*s*, 4*s*–4*p*, and 4*s*–4*p* transitions as seen in figure 1 [61]. Moreover, the peaks corresponding to the N_2 First Positive System are observed at the N band when N_2 is present in the mixture [62].
The OES approach is used in this study to analyze the electron density, degree of dissociation, excitation, vibrational, and rotational temperatures of the DC and RF APJs. The emission intensities of several emission lines are identified from the atomic and molecular transitions. Important characteristics of DC and RF APJs, including electron density, degree of dissociation, electron excitation, and vibrational and rotational temperatures, are ascertained from the acquired data. Furthermore, it should be noted that when one or more of the four temperatures are not equal, the system is said to be in the Partial Local Thermodynamic Equilibrium (PLTE). The electron temperature may be computed using the electron density obtained for the glow and filamentary modes of the plasma jet. However, to analyze the equilibrium, the Saha-Boltzmann equation must be used [63]. The system is strongly collisional for the glow discharges, and the electron density is often estimated at around 1014 cm^{-3}.

Therefore, it may be inferred that the system functions, at minimum, under PLTE conditions [63]. Therefore, in the case of such discharges, if collisional ionizations and radiative recombination are assumed to be the predominant processes in the discharge medium, the PLTE condition between the top levels of each transition is still achievable. Furthermore, one must presume that the source of the plasma discharge is optically thin in the direction of observation. If this approximation is assumed to represent the zeroth order, the absolute emission intensity corresponding to the $a \rightarrow b$ transition may be expressed as follows:

$$I_{ab} = \frac{L}{4\pi} hc \frac{A_{ab} N_a}{\lambda_{ab}} \tag{1}$$

where N_a is the upper-level population of the transition, λ_{ab} is the emission radiation wavelength, L is the plasma dimensional length, h is the Plank constant, c is the light velocity, and A_{ab} is the probability of the transition $a \rightarrow b$, also known as the Einstein coefficient. By considering the plasma discharge systems in the PLTE condition, the Boltzmann distribution relation for the two transitions, $a \rightarrow b$, and $c \rightarrow d$, is often defined as follows:

$$\frac{N_a}{N_c} = \frac{g_a}{g_c} e^{(E_c - E_a)/kT_e} \tag{2}$$

where the energies of levels a and c are represented by E_a and E_c, the statistical weights of levels a and c are represented by g_a and g_c, T_e represents the electron temperature, the Boltzmann constant is represented by k, and N_c is the upper-level population corresponding to the $c \rightarrow d$ transition. To get the species excited density of each level, this equation is rewritten as follows:

$$N_a = \frac{N}{Z} g_a e^{-E_a/kT_e} \tag{3}$$

with N and Z being neutral argon atom density and the canonical partition function. So, the equations 1 and 2 will yield:

$$I_{ab} = \frac{L}{4\pi} hc \frac{N}{Z} \frac{A_{ab} N_a}{\lambda_{ab}} e^{-E_a/kT_e} \tag{4}$$

For any transition line, the slope of $\ln(I\lambda/gA)$ relative to the energy level (E_a) equals $-1/kT_e$, which leads to T_e. It is important to note that, for each transition line in the thermal equilibrium plasma discharges, the plot of $\ln(I\lambda/gA)$ vs the energy level (E_a) is often linear. Furthermore, there is little equilibrium in the plasma discharge at the nozzle exit of the APJ. However, it is often evident that distinct species are recombining in the APJ nozzle. Furthermore, a thorough analysis of the acquired experimental data verifies that the created APJ's plasma discharge is in a situation of partial equilibrium. So, the bound and free electrons mutually in partial equilibrium at the Boltzmann temperature must be included in the appropriate model. Thus, the excited state Saha-Boltzmann equation holds for such a system:

$$n_{SB}(p) = n^+ n_e \frac{g(p)}{2g^+} \left(\frac{h^2}{2\pi m_e k T_e}\right)^{(2/3)} \exp\left(\frac{E_p}{kT_e}\right) \quad p > 2 \tag{5}$$

Since argon is the primary carrier gas in the produced plasma jet, a model for the argon collisional-radiative verifies that when the free electron density is low enough ($< 10^{15} cm^{-3}$), the first excited level population ($p = 2$) begins to diverge from the equilibrium. However, these electrons will go in the direction of the ground-level equilibrium ($p = 1$). Equation 3, where $p > 2$, therefore defines the partial equilibrium model. The partial equilibrium might not be reached until $p > 3$ due to the significant $4p - 4s$ radiative loss [64–66]. This is not expected to happen, though, until the electron density drops below $10^{15} cm^{-3}$. However, this effect is not seen for the evolved APJ.

The resulting spectra are analyzed using the peaks of excited species profiles and the widening of the H_α spectral emission lines for both the produced DC and RF APJs operating with the $Ar/O_2/N_2$ gaseous mixture. Furthermore, using the emission spectra, different species that are associated with the plumes of both jets could be identified. These include O_2^+, NO, and OH molecular emission bands, as well as Ar, N, and O excited atoms. Here, several spectroscopic investigations are performed for the atomic and molecular emission lines to compare the technical and physical properties of the DC and RF APJs as a function of applied power and various $Ar/O_2/N_2$ combinations. It should be mentioned that the kinetic temperatures might be attained by applying the OES approach and figuring out the energy levels of rotationally excited states. It is often considered that the kinetic temperature and rotational temperature at the ground state are in balance. Nonetheless, the distribution of rotational levels is specified by the lifetime of the dipole-allowed transition of the excited states, which is often substantially less than the collision time [67].

In addition, only the N_2^+ $(B^2\Sigma_u^+ - X^2\Sigma_g^+)$ band is chosen for the DC and RF APJs to analyze the resulting rotational temperature. The wavelength of 391.4 nm is the sharp peak of this band. Using LIFBASE software, the simulated curve is fitted to the observed emission spectra in order to determine the rotational temperature (see figure 2) [52]. During the modeling procedure, the emission line shape widening, collisional broadening, and instrumental resolution are taken into account. It is important to remember that there is some degree of error in the rotational temperature calculation due

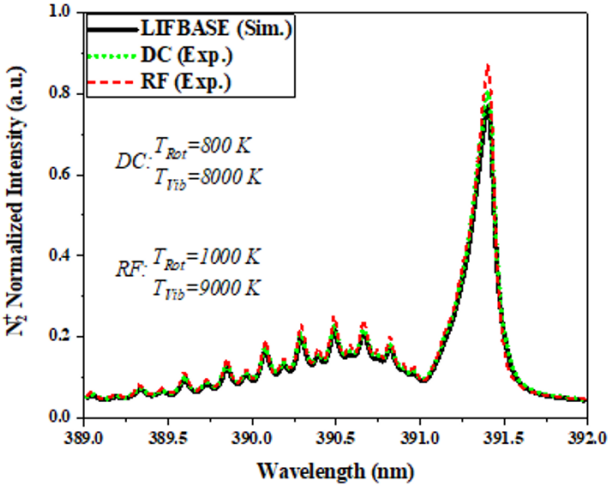

Figure 2. The typical examined rotational and vibrational temperature from the $N_2^+(B^2\Sigma_u^+ - X^2\Sigma_g^+)$ band for 65% Ar at the applied power of 50 W.

to the experimental data′s repeatability and the experimental spectrum data′s adaptability when fitted to the simulated data.

The quantity of excited molecules in a given vibrational state is expressed as the vibrational quantum number, or v. The Boltzmann law defines these states. As a result, the vibrational band′s intensity is as follows [68]:

$$I_{v_1,v_2} = cst.k^4 A(v_1 v_2) e^{\frac{-E_{v_1}}{k_B T}} \quad (6)$$

where v_1 and v_2 are the vibrational quantum numbers of the higher and lower states, respectively. Moreover, E_v is the vibrational energy, k is the wavenumber, and $A(v_1 v_2)$ is the transition probability. It has been demonstrated that if $\ln(\frac{I_{v_1 v_2}}{k^4 A(v_1 v_2)})$ is plotted as a function of E_{v_1}, it should be linear, explaining the vibrational band intensity. The vibrational temperature might be obtained by calculating the slope of such a straight line [68]. It should be mentioned that the validity of the sum rule is contingent upon the transition probability for each vibrational transition that contributes significantly to the total being constant. The temperature of the gas emitting or absorbing the band system may thus be found using the sum rule if this requirement is met. Furthermore, the population of the starting state in thermal equilibrium is proportional to $e^{-E_{v_1}/k_B T}$.

Typically, a nitrogen emission spectrum′s Second Positive System is used to calculate the vibrational temperature of N_2. This suggests that N_2 $(C^3\Pi_u) \rightarrow N_2$ $(B^3\Pi_g)$ is the radiation transition between the C and B electronic states. As a result, the following relation may be used to get the vibrational temperature, T_v:

$$I(C, v' - B, v'') = c(\lambda).[N_2(C, v')].\frac{A(C, v' - B, v'')}{\lambda} \quad (7)$$

where $I(C, v' - B, v'')$ denotes the emission intensity transition between the two energy levels, v' and v'', vibrational numbers. The spectrometer response factor at wavelength λ is represented by the function $c(\lambda)$, the density of nitrogen molecules in the C-state at level v' is represented by $N_2(C, v')$, and the probability of spontaneous emission is represented by $A(C, v' - B, v'')$. It is also possible to represent the density of nitrogen molecules as $[N_2(C, v')] \approx I(C, v' - B, v'').\lambda / A(C, v' - B, v'')$. Lastly, the following method may be used to get the vibrational temperature:

$$N_2(v) = N_2(0)\exp[-hc\frac{G(v)}{kT_v}] \quad (8)$$

By using the logarithm of equation 8, one may derive a linear function against v at the low vibrational levels, which include most vibrationally excited molecules. The slope of the semi-logarithmically plotted population density $(N_2(v_1)/N_2(v_2))$ with the vibrational quantum number, v, yields the vibrational temperature, T_v.

Here, the Boltzmann plot approach is used to quantify the vibrational temperatures in the plume of both the produced DC and RF APJs. Figure 3 displays a typical logarithmic Boltzmann plot showing the relative intensities of the RF APJ distributed according to the vibrational energy state.

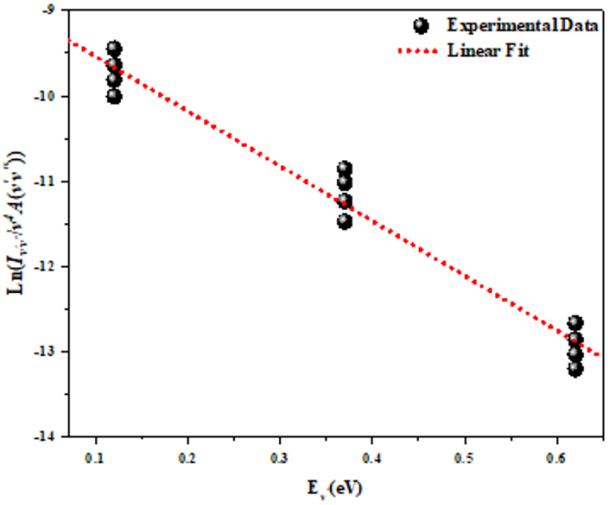

Figure 3. Typical Boltzmann plot of $N_2(C^3\Pi_u \rightarrow B^3\Pi_g)$ vibrational distribution, with $T_{vib} = 10375$ K for the RF APJ.

The dispersed data points are shown here, and the fitting mistakes are considered. Therefore, for the applied power of 50 W and the gaseous mixture ratio of $Ar/O_2/N_2 = 6{:}3{:}1$, respectively, the vibrational temperature is around 10375 K. It is important to note that, for each transition, the vibrational temperature, T_v, is determined by selecting four vibrational bands of N_2 $(C^3\Pi_u \rightarrow B^3\Pi_g)$, namely $\Delta v = 1$, $\Delta v = -1$, $\Delta v = -2$, and $\Delta v = -3$. These correspond to the wavelengths of 315.1 nm, 313.2 nm, 310.8 nm, 349.9 nm, 353.6 nm, 357.6 nm, 370.9 nm, 375.4 nm, 380.4 nm, 394.2 nm, 399.7 nm, and 405.8 nm, respectively. Furthermore, ref. [64] provides the additional parameters.

Many emission lines corresponding to excited argon atoms are seen. Furthermore, these states′ transition probabilities are documented in the published literature. It is possible to determine the excitation temperature at the APJ plume using the standard Boltzmann plot technique. One may argue that in the PLTE condition, the upper and lower levels of the selected atomic transitions are assumed. Thus, it is possible to express the relative transition probabilities of the higher and lower emission levels in the following way [63, 69]:

$$\ln(\frac{I\lambda_{ul}}{A_{ul} g_u}) = \ln(\frac{hcN_0}{4\pi U(t)}) - \frac{E_u}{kT_{exc}} \quad (9)$$

where g_u is the higher level′s degeneracy, E_u is the upper level′s excitation energy, I is the total intensity, k is the Boltzmann constant, and λ_{ul} and A_{ul} are the wavelength difference and transition probability between the upper and lower levels, respectively. It is important to remember that electron effects are often overcome during the populating and depopulating processes between excited atoms. It should be noted that a Boltzmann approach is used to drive the slope of the fitted line to calculate the excitation temperature of the APJ. Equation 9 and the selected argon atom emission lines are used to depict $\ln(\frac{I\lambda_{ul}}{A_{ul} g_u})$ as a function of upper-level excitation energy E_u. Here, the necessary values for the argon atom emission lines are extracted using the National Institute of Standards and Technology (NIST)

database [70].

Furthermore, we may assume that the electrically excited neutrals are in quasi-equilibrium with plasma electrons in order to compute the maximal stepwise ionization rate. Furthermore, the Boltzmann distribution with electron temperature T_e describes the electrically excited states in the following way:

$$N_n = (\frac{g_n}{g_0})N_0 \exp(-\frac{\varepsilon_n}{T_e}) \tag{10}$$

The index n is the primary quantum number, N_n is the number densities, g_n is statistical weights, and ε_n is the energy of the electronically excited atoms, radicals, or molecules. The statistical weight of an excited particle is given by $g_n = 2g_i n^2$, where g_i is the statistical weight of an ion, according to statistical thermodynamics. The concentration and statistical weights of ground-state particles are denoted by N_0 and g_0. The typical energy transfer from a plasma electron to another electron is denoted by T_e. Therefore, equation 10 primarily involves excited particles with energies of around $\varepsilon_n = I - T_e$. In the case when $I_n \sim 1/n^2$, there are n states with energies approximately equal to $\varepsilon_n = I - T_e$ and an ionization potential approximately equal to $I_n = T_e$. Thus, the following relationship may be inferred from equations 10:

$$k \approx (\frac{g_i}{g_0})n^3 < \sigma v > \exp(-\frac{1}{T_e}) \tag{11}$$

Ultimately, $e^4/(T_e^2(4\pi\varepsilon_0)^2)$ may be used to determine the cross-section σ in the preceding equation, which represents an energy transfer of about T_e between electrons [39].

Figure 4 displays the rotational, vibrational, and excitation temperatures for both the DC and RF APJs as a function of the input DC and RF powers and the argon contribution in the $Ar/O_2/N_2$ gaseous mixture. The rotational temperatures of DC and RF APJs range from $750-900$ K and $950-1100$ K, respectively, as shown in figure 4(a). The distribution of the molecular rotational states is generally correlated with the rotational temperature. Furthermore, the lifespan of the N_2^+ radical in the excited state is longer than the rotating levels′ relaxation duration, which is just a few nanoseconds [56]. In contrast, the collision frequency is noticeably high at atmospheric pressures. Therefore, there is enough time to allow the excited molecules and gas particles to come into balance before the instantaneous photon emission. As

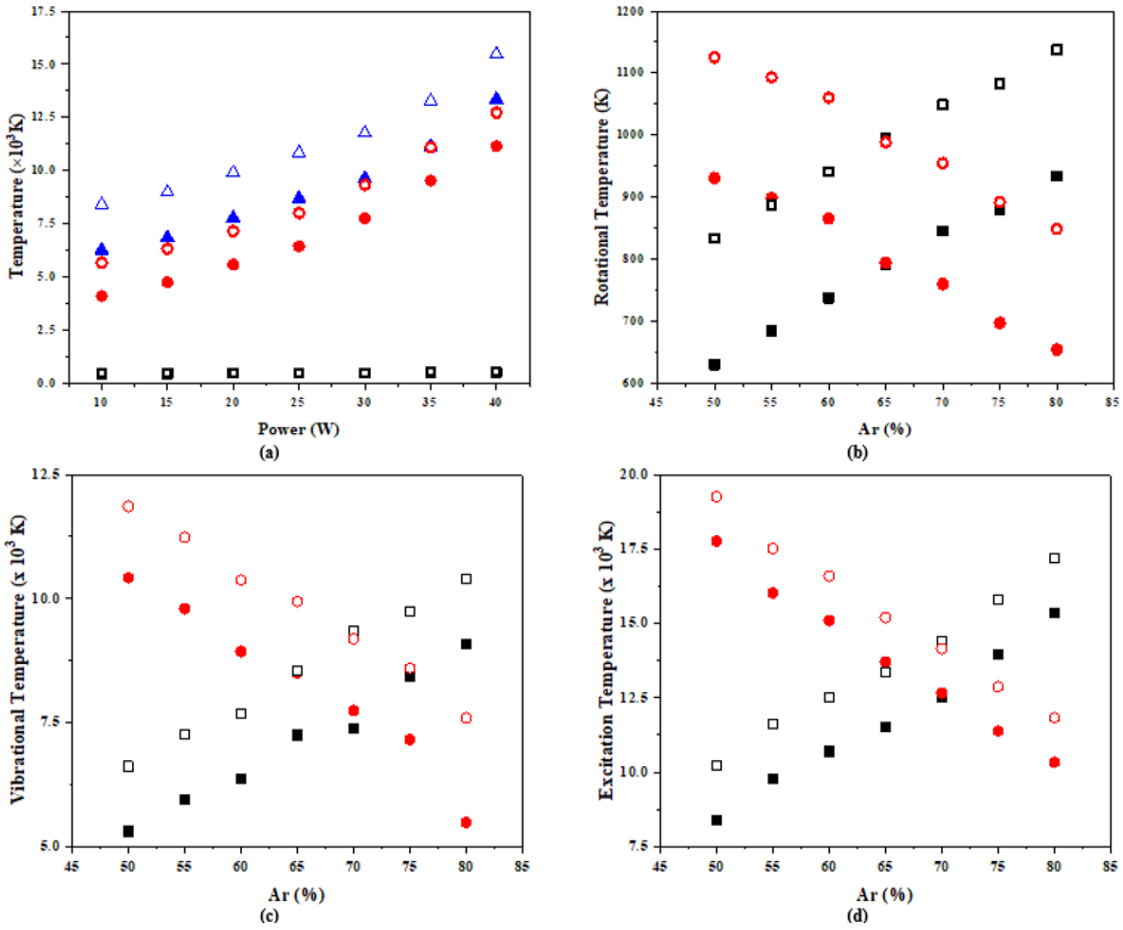

Figure 4. (a) Variations of all the measured temperatures for DC (■ rotation, . vibration and ▲excitation temperatures) and RF (□ rotation, ○ vibration and Δ excitation temperatures) APJs as a function of DC and RF electrical powers with Ar:O_2:N_2 (6:3:1) (b) Rotational temperature as a function of Ar percentages in the $Ar/O_2/N_2$ gaseous mixture with various O_2/N_2 ratios (increase with step of 0.5) for DC (■ O_2:N_2 (1:4), . O_2:N_2 (4:1)) and RF (□ O_2:N_2 (1:4), ○ O_2:N_2 (4:1)), (c) Vibrational temperature as a function of Ar percentages in the $Ar/O_2/N_2$ gaseous mixture with various O_2/N_2 ratios (increase with step of 0.5) for DC (■ O_2:N_2 (1:4), . O_2:N_2 (4:1)) and RF (□ O_2:N_2 (1:4), ○ O_2:N_2 (4:1)), (d) Excitation temperature as a function of Ar percentages in the $Ar/O_2/N_2$ gaseous mixture with various O_2/N_2 ratios (increase with step of 0.5) for DC (■ O_2:N_2 (1:4), . O_2:N_2 (4:1)) and RF (□ O_2:N_2 (1:4), ○ O_2:N_2 (4:1)).

a result, the rotational temperature and the temperature of the gas molecules in plasma discharges are comparable [54]. Moreover, the energy magnitude between the two normal rotational levels is nearly identical to the neutral species′ kinetic energy. Moreover, the inelastic collisions between the heavier species in the molecular plasma can generate a large change in the rotational quantum number. As a result, the collisions of the heavier particles with the molecules sustain rotational energy transfer at rather high rotational levels. When compared to atomic plasmas, such low-energy exchanges are insignificant [58]. As a result, it is practically simpler to measure the greater rotational temperature in atomic plasmas than in molecular plasmas. Consequently, N_2^+ ($B^2\Sigma_u^+ - X^2\Sigma_g^+$) rotational temperature in molecular gas plasmas gives sufficient information on the temperature of heavy species in the generated plasma discharge. It is important to note that the equivalent rotational temperature for the N_2^+ ($B^2\Sigma_u^+ - X^2\Sigma_g^+$) transition in atomic plasma discharges is extremely near to the gas temperature at atmospheric pressures. Furthermore, the excitation and vibrational temperatures are raised, as seen in figure 4(a). Nevertheless, this is because the ionization process by the plasma electrons is directly impacted by the greater input of DC and RF electrical energy into the discharge medium of APJs. Moreover, the electron density increases with increasing DC and RF powers. The ionization process involving argon metastable species hence has a larger Penning effect. As seen in figure 4(b), in this case, the argon contribution will not affect the gas temperature for the $Ar/O_2/N_2$ gaseous combination from the First Positive System. On the other hand, the wavelengths of the Second Positive System diverge. It is possible to compute the rotational temperature using these. However, the temperature derived from the Second Positive peak is greater compared to the First Positive peak.

Furthermore, the argon metastable atoms get an effective energy transfer from the ground state of nitrogen, which starts the extreme overcrowding of the rotating levels. As a result, when the First Positive System is applied, the computed rotational temperatures are substantially higher than those obtained using this approach. Figure 4(c) displays the vibrational temperature derived from the nitrogen Second Positive System in the DC and RF APJs with the gaseous combination of $Ar/O_2/N_2$. It may be observed that when N_2 contributes more than O_2, Tv rises as argon percentages in the mixture do. Additionally, as figure 4(c) illustrates, when the O_2 contribution in the mixture exceeds the N_2 contribution, the vibrational temperature drops at the bigger argon contributions. This is because, at higher argon percentages in the $Ar/O_2/N_2$ gas mixture, the pooling reactions and electron collisions ratio between the oxygen and metastable species of argon atoms are decreased [71, 72].

As can be seen in figure 4(d), the excitation temperature rises at the greater argon contributions in the $Ar/O_2/N_2$ gaseous mixture when the O_2/N2 fraction is less than one. The reason for this is that argon has a smaller electron collision cross section than molecular nitrogen. Because of this, the energetic electrons may smash with the nitrogen molecules directly, causing the molecules to become excited and ionized. Furthermore, by striking argon-neutral atoms at the ground state, they may produce argon metastable species. Consequently, the argon atom and target species can experience both excitation and ionization processes as a result of ionization and excitation processes. Furthermore, the ionization-related nitrogen cross-sections are around $\sim 2.5 \times 10^{-20} m^2$, which is close to the argon atoms [73]. Therefore, if argon atoms are present in the discharge region of both DC and RF APJs, these characteristics cannot account for the observed elevation in the excitation temperature. Nonetheless, the primary cause of the elevated electron temperature is associated with the energetic electrons in the tail of the EEDF and their noteworthy impacts on ionizing collisions inside the jet discharge medium. Furthermore, compared to typical excited states, the electron lifetime in metastable states is much shorter [74]. Moreover, raising the argon contributions in the $Ar/O_2/N_2$ mixture will result in a drop in the excitation temperature when the O_2 contribution in the mixture is greater than the N_2 contribution. However, the energy lost by the electrons during their interaction with oxygen molecules decreases because the oxygen ionization process has a lower cross-section than argon [72]. Its exothermic dissociation reaction ratio also falls as the O_2 contribution does. As a result, the temperature of the electrons drops.

Due to its good approximation and straightforward approach, the Stark broadening method works well for measuring the electron density in plasma jets. This widening, which is based on the Stark effect, is brought about by the emitting atoms′ Coulomb interaction with free electrons and ions in the plasma via the electrical field. Therefore, if the electron temperature is known, the Stark broadening of a particular spectral line that is spontaneously released by plasma particles may be used to quickly and conveniently measure the electron density. Most often, the electron density in atmospheric pressure plasma was found using the Stark broadening of the Balmer line [75]. The fine structure and ion dynamics concerns are not necessary in this technique [76]. In addition, the Full-Width at Half-Maximum (FWHM) parameter is widely used to determine the emission line shape broadening. The Stark broadening is influenced by the FWHM values.

In this work, the H_α line at 656 nm could be found in emission spectra. The Stark broadening ($\Delta\lambda_S$) may be used to estimate the electron density (n_e) in the plasma discharge region of the DC and RF APJs as follows [75, 77]:

$$\Delta\lambda_s = 2 \times 10^{-11} (n_e^{2/3}) \tag{12}$$

Therefore, electron density in plasma discharge is calculated in cm^{-3} units based on knowledge of the Stark broadening [78]. Next, the following relation might be used to express Stark broadening reliance on the Lorentz $\Delta\lambda_L$ and van der Waals broadenings $\Delta\lambda_v$ [79]:

$$\Delta\lambda_L = \Delta\lambda_s + \Delta\lambda_v \tag{13}$$

However, the disruption in the energy states of the emitting species causes the pressure to expand because neutral species are present in the discharge region of the DC and RF APJs. The Lorentzian profile is a result of this broadening′s

relationship to resonance and van der Waals broadening. The density of hydrogen atoms in the ongoing studies is noticeably low. Therefore, only the van der Waals broadening is considered. Thus, the van der Waals profile′s FWHM is expressed as follows [79–81]:

$$\Delta\lambda_v = 3.6 \times \frac{P}{T^{0.7}} \tag{14}$$

with p and T being the pressure and temperature in atm and K units, respectively. Furthermore, the Doppler profile is dependent on the Gaussian broadening which could be given by [82]:

$$\Delta\lambda_D\ (\text{nm}) = 7.2 \times 10^{-7} \sqrt{\frac{T}{M}}\lambda \tag{15}$$

where λ stands for the wavelength (= 656 nm), M is hydrogen weight (= 1 g/mol), and T denotes the temperature which is usually equal to the gas temperature. In order to obtain the Voigt profile, the important broadenings which must be considered are given as [72]:

$$\Delta\lambda_G = \sqrt{\Delta\lambda_D^2 + \Delta\lambda_{GI}^2} \tag{16}$$

here, $\Delta\lambda_G$ represents the Gaussian broadening and $\Delta\lambda_{GI}$ stands for the instrumental broadening with a Gaussian shape related to the resolution of the optical instruments of the spectrometer directly. Furthermore, a superposition approach is employed to ascertain the Voigt profile using the Gaussian and Lorentzian profiles. To determine the Lorentz broadening, the experimental spectrum might be fitted using the Voigt Profile. However, the same spectrum analysis technique is done by the Origin software in order to estimate the FWHM of Lorentzian broadening. Thus, the resulting Lorentzian and van der Waals broadenings may be used to establish the Stark profile that leads to the electron density.

The changes in plasma electron density with the input DC and RF electrical powers as well as the proportion of Ar in the $Ar/O_2/N_2$ gaseous mixture are depicted in figure 5. The electron density rises with the input DC and RF powers, as seen in figure 5(a). It should be mentioned that when both the DC and RF electrical powers are larger, the input electrical power to the discharge region increases. As a result, the ionization rate rises and there are stronger electric fields inside the discharge medium. However, argon atoms rather than oxygen molecules can be ionized during the processes of ionization by plasma-charged species. Furthermore, the electron attachment in the plasma discharge region decreases with decreasing oxygen contributions in the $Ar/O_2/N_2$ gaseous mixture. Moreover, there are greater energy losses in the activation of vibrational modes at increasing oxygen contributions in the $Ar/O_2/N_2$ combination [71]. As a result, in the $Ar/O_2/N_2$ gaseous mixture, the plasma electron density rises in relation to the Ar percentages as seen in figure 5(b). Furthermore, the plasma electron density decreases with increasing N_2 contribution in the gas mixture at bigger Ar contributions in the $Ar/O_2/N_2$ combination. Thus, the rate at which molecular nitrogen dissociates will be slowed down by the drop in plasma electron density. It is true that when the argon contribution in the $Ar/O_2/N_2$ gas mixture increases, the likelihood of Ar metastable production increases. So, $N_2(C^3\Pi_u)$ will produce at a higher pace. The decrease in spectral intensities at the greater argon contributions in the gaseous mixture is the cause of this. Moreover, this phenomenon signifies a decrease in molecular dissociation.

One important characteristic in molecular gaseous plasma discharges is the dissociation rate for molecular gases, such as oxygen and nitrogen. However, the dissociation rate of these molecular gases may be accelerated by the presence of an extra gas, such as hydrogen or argon. Atomic densities at the molecular plasma discharge region are often characterized in both qualitative and quantitative forms using the actinometry method, which is based on the OES technique when an inert gas is supplied. In this case, the optical emission actinometry is performed using three spectral emission lines: argon (wavelength of 750 nm), nitrogen (wavelength of 672 nm), and oxygen (wavelength of 777 nm). As a result, the following dissociation fraction rates

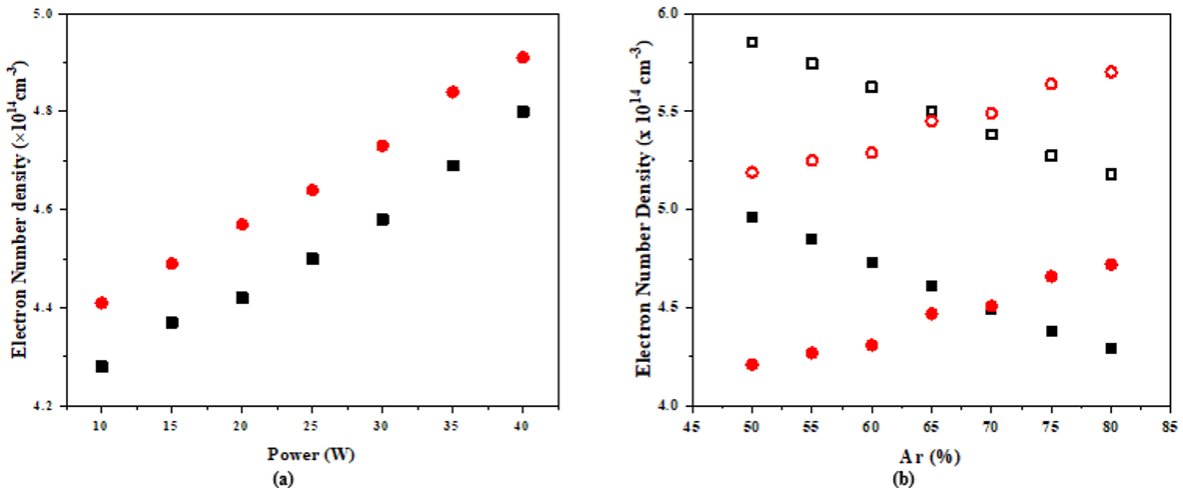

Figure 5. Evolution of the plasma electron density as a function of (a) ■ DC and . RF electrical powers at $Ar/O_2/N_2$ (6:1:3), (b) Ar percentages in the $Ar/O_2/N_2$ gaseous mixture with various O_2/N_2 ratios (with step of 0.5) for DC (■ O_2:N_2 (1:4), . O_2:N_2 (4:1)) and RF (□ O_2:N_2 (1:4), ○ O_2:N_2 (4:1)).

may be found [83]:

$$\frac{[O]}{[O_2]} = C_1 \left\{ \frac{[Ar]}{[O_2]} \right\} \frac{I_O}{I_{Ar}} \frac{K(\lambda_{777})}{K(\lambda_{750})} \quad (17)$$

$$\frac{[N]}{[N_2]} = C_2 \left\{ \frac{[Ar]}{[N_2]} \right\} \frac{I_N}{I_{Ar}} \frac{K(\lambda_{672})}{K(\lambda_{750})} \quad (18)$$

where I_N, I_O, and I_{Ar} denote the intensities of the atomic nitrogen, oxygen, and argon emission lines at the corresponding wavelengths of 672.3 nm, 777 nm, and 750.4 nm. When the plasma discharge is off, the initial ratios of Ar/N_2 and Ar/O_2 percentages are $\{[Ar]/[N_2]\}$ and $\{[Ar]/[O_2]\}$. Spectral responses $K(\lambda_{750})$, $K(\lambda_{777})$, and $K(\lambda_{672})$ are also identified based on the argon, oxygen, and nitrogen emission lines, respectively. Furthermore, the constants for C_1 and C_2 were associated with significant spectroscopic information [84].

Figure 6 displays the dissociation fraction of nitrogen and oxygen atoms into the $Ar/O_2/N_2$ gaseous mixture as a function of Ar percentages for both DC and RF APJs at 777 nm and 672 nm wavelengths. As can be seen, the dissociation fraction increases as the Ar component in the $Ar/O_2/N_2$ gaseous mixture increases. The actinometry for plasma discharges with greater Ar contributions in the mixture results in an overestimation of the dissociation fraction. However, this is due to the Penning excitation of O and N atoms by excited argon atoms at the discharge region of the DC and RF APJs [85, 86].

4. Conclusion

In this study, the impact of adding atomic argon to the O_2/N_2 plasma in the DC and RF APJs was investigated using the OES technique. The experimental work involved calculating plasma density and rotational, vibrational, and excitation temperatures. The intensity of NO γ emission lines, which represent electronic transitions, was greater in the RF APJ than in the DC one. It was demonstrated that as the argon component to the $Ar/O_2/N_2$ gaseous mixture grew, so did the intensity of Ar I emissions. Furthermore, the vibrational and excitation temperatures rise as the input power increases whereas the rotational temperature remains almost constant with DC and RF powers. Once the amount of oxygen exceeds the amount of nitrogen, the vibrational and excitation temperatures fall. On the contrary, the vibrational and excitation temperatures rise when nitrogen contributes more than oxygen. Furthermore, the density of plasma electrons rises with increasing DC and RF power. If the Ar percentage of the gas mixture increases and the amount of molecular nitrogen exceeds that of oxygen, the electron density decreases. It is, however, boosted when the oxygen input exceeds that of nitrogen. Greater Ar percentages in the mixture resulted in increased dissociation fractions of oxygen and nitrogen molecules. It is possible to deduce that as the oxygen contribution in the $Ar/O_2/N_2$ combination increases, so does the gas temperature for the RF APJ, making it acceptable for medical applications such as surgery. If the nitrogen contribution in the $Ar/O_2/N_2$ combination is higher, the DC APJ operates at a lower temperature than the RF one which makes it appropriate for biological applications like decontamination and sterilization.

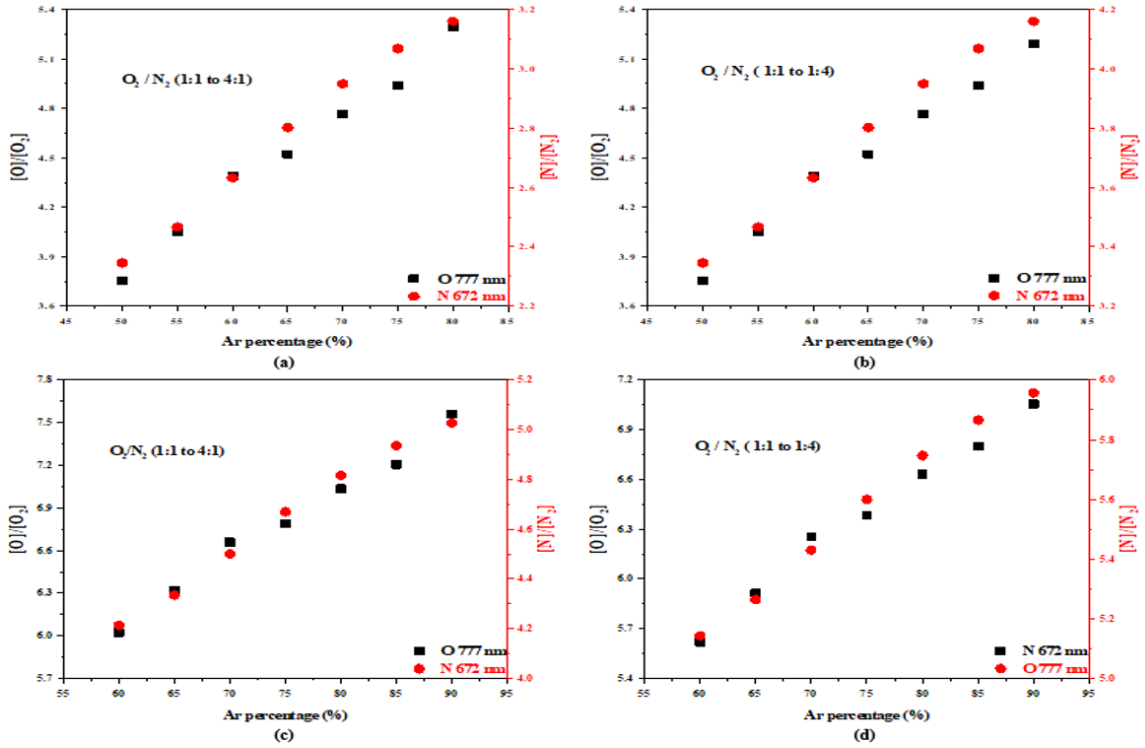

Figure 6. Evolution of O_2 and N_2 dissociation fraction in the plasma discharge medium as a function of Ar percentages for (a, b) DC and (c, d) RF APJs. The O_2/N_2 ratio increases with the steps of 0.5.

Authors Contribution
All the authors have participated sufficiently in the intellectual content, conception and design of this work or the analysis and interpretation of the data (when applicable), as well as the writing of the manuscript.

Availability of data and materials
The datasets used and/or analyzed during the current study are available from the corresponding author upon reasonable request.

Conflict of interests
The authors declare no financial or commercial conflict of interest.

References

[1] M. Moisan, J. Barbeau, J. Moreau, S. Pelletier, M. Tabrizian, and Y. L'H. "Low-temperature sterilization using gas plasmas: a review of the experiments and an analysis of the inactivation mechanisms. ". *International journal of Pharmaceutics.*, **226**(1-2):1–21, 2001.
DOI: https://doi.org/10.1016/S0378-5173(01)00752-9.

[2] S. Lerouge, M. R. Wertheimer, and L. H. Yahia. "Plasma sterilization: a review of parameters, mechanisms, and limitations.". *Plasmas and polymers*, **6**:175–88, 2001.
DOI: https://doi.org/10.1023/A:1013196629791.

[3] T. C. Montie, K. Kelly-Wintenberg, and J. R. Roth. "An overview of research using the one atmosphere uniform glow discharge plasma (OAUGDP) for sterilization of surfaces and materials.". *IEEE Transactions on plasma science*, **28**(1):41–50, 2000.
DOI: https://doi.org/10.1109/27.842860.

[4] M. Laroussi. "Low temperature plasma-based sterilization: overview and state-of-the-art. ". *Plasma processes and polymers*, **2**(5):391–400, 2005.
DOI: https://doi.org/10.1002/ppap.200400078.

[5] F. Rossi, O. Kylian, and M. Hasiwa. "Decontamination of surfaces by low pressure plasma discharges.". *Plasma Processes and Polymers*, **3**(6-7):431–42, 2006.
DOI: https://doi.org/10.1002/ppap.200600011.

[6] A. Barkhordari, S. Karimian, A. Rodero, D. A. Krawczyk, S. I. Mirzaei, and A. Falahat. "Carbon dioxide decomposition by a parallel-plate plasma reactor: Experiments and 2-D modelling. ". *Applied Sciences*, **11**(21):10047, 2021.
DOI: https://doi.org/10.3390/app112110047.

[7] A. Von Keudell, P. Awakowicz, J. Benedikt, V. Raballand, A. Yanguas-Gil, J. Opretzka, C. Flotgen, R. Reuter, L. Byelykh, H. Halfmann, and K. Stapelmann. "Inactivation of bacteria and biomolecules by low-pressure plasma discharges.". *Plasma Processes and Polymers*, **7**(3-4):327–52, 2010.
DOI: https://doi.org/10.1002/ppap.200900121.

[8] H. Yu, Z. L. Xiu, C. S. Ren, J. L. Zhang, D. Z. Wang, Y. N. Wang, and T. C. Ma. "Inactivation of yeast by dielectric barrier discharge (DBD) plasma in helium at atmospheric pressure.". *IEEE transactions on plasma science*, **33**(4):1405–9, 2005.
DOI: https://doi.org/10.1109/TPS.2005.851961.

[9] A. Barkhordari, S. I. Mirzaei, A. Falahat, and A. Rodero. "Numerical and experimental study of an Ar/CO_2 plasma in a point-to-plane reactor at atmospheric pressure.". *Spectrochimica acta part B: Atomic spectroscopy.*, **177**:106048, 2021.
DOI: https://doi.org/10.1016/j.sab.2020.106048.

[10] O. Kylian, M. Hasiwa, and F. Rossi. " Effect of low-pressure microwave discharges on pyrogen bioactivity.". *IEEE transactions on plasma science*, **34**(6):2606–10, 200.
DOI: https://doi.org/10.1109/TPS.2006.885093.

[11] M. Hasiwa, O. Kylian, and F. Hartung, T. Rossi. "Removal of immune-stimulatory components from surfaces by plasma discharges.". *Innate Immunity*, **14**(2):89–97, 2008.
DOI: https://doi.org/10.1177/175342590708.

[12] H. C. Baxter, G. A. Campbell, A. G. Whittaker, A. C. Jones, A. Aitken, A. H. Simpson, M. Casey, L. Bountiff, L. Gibbard, and R. L. Baxter. "Elimination of transmissible spongiform encephalopathy infectivity and decontamination of surgical instruments by using radio-frequency gas-plasma treatment. ". *Journal of general virology*, **86**(8):2393–9, 2005.
DOI: https://doi.org/10.1099/vir.0.81016-0.

[13] H. C. Baxter, P. R. Richardson, G. A. Campbell, V. I. Kovalev, R. Maier, J. S. Barton, A. C. Jones, G. DeLarge, M. Casey, and R. L. Baxter. " Application of epifluorescence scanning for monitoring the efficacy of protein removal by RF gas–plasma decontamination.". *New Journal of Physics*, **11**(11):115028, 2009.
DOI: https://doi.org/10.1088/1367-2630/11/11/115028.

[14] X. T. Deng, J. J. Shi, and M. G. Kong. "Protein destruction by a helium atmospheric pressure glow discharge: capability and mechanisms.". *Journal of applied physics*, **101**(7), 2007.
DOI: https://doi.org/10.1063/1.2717576.

[15] G. Ceccone, D. Gilliland, O. Kylian, and F. Rossi. " Experimental study of effect of low-pressure O_2: H_2 microwave discharge on protein films.". *Czechoslovak Journal of Physics*, **56**:B672–7, 2006.
DOI: https://doi.org/10.1007/s10582-006-0269-1.

[16] S. Karimian, S. Falahat, Z. E. Bakhsh, M. J. Rad, and A. Barkhordari. "A comparative study on predicting the characteristics of plasma activated water: artificial neural network (ANN) & support vector regression (SVR).". *Journal of Theoretical and Applied Physics*, **18** (4), 2024.
DOI: https://doi.org/10.57647/j.jtap.2024.1804.48.

[17] A. Barkhordari, S. Karimian, S. Shahsavari, D. Krawczyk, and A. Rodero. "Influence of the argon admixture on the reactive oxide species formation inside an atmospheric pressure oxygen plasma jet.". *Scientific Reports*, **14**(1):3425, 2024.
DOI: https://doi.org/10.1038/s41598-024-54111-y.

[18] K. Stapelmann, O. Kylian, B. Denis, and F. Rossi. "On the application of inductively coupled plasma discharges sustained in Ar/O2/N2 ternary mixture for sterilization and decontamination of medical instruments.". *Journal of Physics D: Applied Physics.*, **41**(19):192005, 2008.
DOI: https://doi.org/10.1088/0022-3727/41/19/192005.

[19] O. Kylian and F. Rossi. "Sterilization and decontamination of medical instruments by low-pressure plasma discharges: application of Ar/O_2/N_2 ternary mixture.". *Journal of Physics D: Applied Physics.*, **42**(8):085207, 2009.
DOI: https://doi.org/10.1088/0022-3727/42/8/08520.

[20] N. Munakata, K. Hidea, K. Kobayashi, A. Ito, and T. Ito. "Action spectra in ultraviolet wavelengths (150-250 nm) for inactivation and mutagenesis of bacillus subtilis spores obtained with synchrotron radiation.". *Photochemistry and photobiology*, **44**(3):385–90, 1986.
DOI: https://doi.org/10.1111/j.1751-1097.1986.tb04680.x.

[21] M. K. Boudam and M. Moisan. "Synergy effect of heat and UV photons on bacterial-spore inactivation in an N_2–O_2 plasma-afterglow sterilizer.". *Journal of physics D: applied physics.*, **43**(29):295202, 2010.
DOI: https://doi.org/10.1088/0022-3727/43/29/295202.

[22] Y. Yasuda, S. Zaima, T. Kaida, and Y. Koide. "Mechanisms of silicon oxidation at low temperatures by microwave-excited O_2 gas and O_2-N_2 mixed gas. ". *Journal of applied physics*, **67**(5):2603–7, 1990.
DOI: https://doi.org/10.1063/1.345465.

[23] A. Vesel, M. Kolar, N. Recek, K. Kutasi, K. Stana-Kleinschek, and M. Mozetic. "Etching of blood proteins in the early and late flowing afterglow of oxygen plasma.". *Plasma Processes and Polymers*, **11** (1):12–23, 2014.
DOI: https://doi.org/10.1002/ppap.201300067.

[24] K. Kutasi, C. Noel, T. Belmonte, and V. Guerra. "Tuning the afterglow plasma composition in Ar/N_2/O_2 mixtures: characteristics of a flowing surface-wave microwave discharge system.". *Plasma Sources Science and Technology*, **25**(5):055014, 2016.
DOI: https://doi.org/10.1088/0963-0252/25/5/055014.

[25] S. Greenfield, P. B. Smith, H. M. McGeachin, R. M. Dagnall, B. L. Sharp, and D. R. Marriott. " Plasma excitation in spectrochemical analysis.". *Proceedings of the Society for Analytical Chemistry*, **10** (4):89–91, 1973.
DOI: https://doi.org/10.1039/SA9731000089.

[26] Bessoth F. G., O. P. Naji, J. C. Eijkel, and A. Manz. "Towards an on-chip gas chromatograph: the development of a gas injector and a dc plasma emission detector.". *Journal of Analytical Atomic Spectrometry*, **17**(8):794–9, 2002.
DOI: https://doi.org/10.1039/B203180A.

[27] C. G. Wilson and Y. B. Gianchandani. "Spectral detection of metal contaminants in water using an on-chip microglow discharge.". *IEEE Transactions on Electron Devices*, **49**(12):2317–22, 2002.
DOI: https://doi.org/10.1109/TED.2002.805608.

[28] J. Franzke, K. Kunze, M. Miclea, and K. Niemax. "Microplasmas for analytical spectrometry.". *Journal of Analytical Atomic Spectrometry*, **18**(7):802–7, 2003.
DOI: https://doi.org/10.1039/B300193H.

[29] F. J. Andrade, W. C. Wetzel, G. C. Chan, M. R. Webb, G. Gamez, S. J. Ray, and G. M. Hieftje. "A new, versatile, direct-current helium atmospheric-pressure glow discharge.". *Journal of analytical atomic spectrometry*, **21**(11):1175–84, 2006.
DOI: https://doi.org/10.1039/B607544D.

[30] A. Barkhordari, A. Ganjovi, I. Mirzaei, A. Falahat, and M. N. Rostami Ravari. "A pulsed plasma jet with the various Ar/N_2 mixtures. ". *Journal of Theoretical and Applied Physics*, **11**:301–12, 2017.
DOI: https://doi.org/10.1007/s40094-017-0271-y.

[31] A. Barkhordari, A. Ganjovi, I. Mirzaei, and A. Falahat. "Study of the physical discharge properties of a Ar/O 2 DC plasma jet. ". *Indian Journal of Physics*, **92**:1177–86, 2018.
DOI: https://doi.org/10.1007/s12648-018-1197-1.

[32] A. Barkhordari and A. Ganjovi. "Technical characteristics of a DC plasma jet with Ar/N_2 and O_2/N_2 gaseous mixtures.". *Chinese Journal of Physics*, **57**:465–78, 2019.
DOI: https://doi.org/10.1016/j.cjph.2018.10.017.

[33] A. Falahat, A. Ganjovi, M. Taraz, M. R. Ravari, and A. Shahedi. " Optical characteristics of a RF DBD plasma jet in various Ar/O_2 mixtures.". *Pramana*, **90**(2):27, 2018.
DOI: https://doi.org/10.1007/s12043-018-1520-6.

[34] A. Barkhordari, A. Ganjovi, and S. I. Mirzaei. "Experimental study of a positive DC corona jet working with Ar/CO_2 gaseous mixture.". *Pramana*, **95**:1–3, 2021.
DOI: https://doi.org/10.1007/s12043-021-02090-4.

[35] A. Morisako, M. Matsumoto, S. Takei, and T. Yamazaki. "Effect of substrate temperature on magnetic properties of strontium ferrite thin films.". *IEEE Transactions on Magnetics.*, **33**(5):3100–2, 1997.
DOI: https://doi.org/10.1109/20.617857.

[36] J. Zhang, X. Li, W. Yang, W. Yan, D. Wei, Y. Liu, and G. Yan. "The effect of the length to diameter ratio on capillary discharge plasmas.". *Physics of Plasmas*, **25**(10), 2018.
DOI: https://doi.org/10.1063/1.5041781.

[37] C. Tendero, C. Tixier, P. Tristant, J. Desmaison, and P. Leprince. "Atmospheric pressure plasmas: A review. ". *Spectrochimica Acta Part B: Atomic Spectroscopy.*, **61**(1):2–30, 2006.
DOI: https://doi.org/10.1016/j.sab.2005.10.003.

[38] H. X. Deng, X. L. Gong, and L. H. Wang. "Development of an adaptive tuned vibration absorber with magnetorheologicalelastomer.". *Smart materials and structures*, **15**(5):N111, 2006.
DOI: https://doi.org/10.1088/0964-1726/15/5/N02.

[39] A. Fridman and G. Friedman. "Plasma Medicine". *Begell House, US,*, **1**:21, 2010.

[40] J. S. Chang, P. A. Lawless, and T. Yamamoto. "Corona discharge processes. ". *IEEE Transactions on plasma science*, **19**(6):1152–66, 1991.
DOI: https://doi.org/10.1109/27.125038.

[41] F. Grum and L. F. Costa. "Spectral emission of corona discharges.". *Applied Optics*, **15**(1):76–9, 1976.
DOI: https://doi.org/10.1364/AO.15.000076.

[42] M. Goldman, A. Goldman, and R. S. Sigmond. "The corona discharge, its properties and specific uses.". *Pure and Applied Chemistry*, **57**(9):1353–62, 1985.
DOI: https://doi.org/10.1351/pac198557091353.

[43] A. Barkhordari, S. I. Mirzaei, A. Falahat, D. A. Krawczyk, and A. Rodero. "Experimental study of a rotating electrode plasma reactor for hydrogen production from liquid petroleum gas conversion.". *Applied Sciences*, **12**(8):4045, 2022.
DOI: https://doi.org/10.3390/app12084045.

[44] Z. Weiss. "Quantitative depth profile analysis by glow discharge optical emission spectrometry: an alternative approach. ". *Journal of Analytical Atomic Spectrometry*, **10**(10):891–5, 1995.
DOI: https://doi.org/10.1039/JA9951000891.

[45] K. Hensel, S. Katsura, and A. Mizuno. "DC microdischarges inside porous ceramics. ". *IEEE Transactions on Plasma Science*, **33**(2): 574–5, 2005.
DOI: https://doi.org/10.1109/TPS.2005.845389.

[46] Z. Machala, M. Janda, K. Hensel, I. Jedlovsky, L. Lestinska, V. Foltin, V. Martisovits, and M. Morvova. "Emission spectroscopy of atmospheric pressure plasmas for bio-medical and environmental applications.". *Journal of Molecular Spectroscopy*, **243**(2):194–201, 2007.
DOI: https://doi.org/10.1016/j.jms.2007.03.001.

[47] K. Shimizu and T. Oda. "Emission spectrometry for discharge plasma diagnosis. ". *Science and Technology of Advanced Materials*, **2**(3-4): 577, 2001.
DOI: https://doi.org/10.1016/S1468-6996(01)00140-1.

[48] L. G. Piper, L. M. Cowles, and W. T. Rawlins. "State-to-state excitation of NO ($A_2\sum+$, v′= 0, 1, 2) by N_2(A $3\sum+$ u, v′= 0, 1, 2).". *The Journal of chemical physics*, **85**(6):3369–78, 1986.
DOI: https://doi.org/10.1063/1.450958.

[49] Z. Machala, M. Morvova, E. Marode, and I. Morva. "Removal of cyclohexanone in transition electric discharges atatmospheric pressure.". *Journal of Physics D: Applied Physics*, **33**(24):3198, 2000.
DOI: https://doi.org/10.1088/0022-3727/33/24/313.

[50] D. Nie, W. Wang, D. Yang, H. Shi, Y. Huo, and L. Dai. "Optical study of diffuse bi-directional nanosecond pulsed dielectric barrier discharge in nitrogen.". *Spectrochimica Acta Part A: Molecular and Biomolecular Spectroscopy.*, **79**(5):1896–903, 2011.
DOI: https://doi.org/10.1016/j.saa.2011.05.083.

[51] P. Bruggeman, F. Iza, P. Guns, D. Lauwers, M. G. Kong, Y. A. Gonzalvo, C. Leys, and D. C. Schram. "Electronic quenching of OH (A) by water in atmospheric pressure plasmas and its influence on the gas temperature determination by OH (A–X) emission.". *Plasma Sources Science and Technology.*, **19**(1):015016, 2009.
DOI: https://doi.org/10.1088/0963-0252/19/1/015016.

[52] A. Bogaerts and R. Gijbels. "Fundamental aspects and applications of glow discharge spectrometric techniques.". *Spectrochimica Acta Part B: Atomic Spectroscopy*, **53**(1):1–42, 1998.
DOI: https://doi.org/10.1016/S0584-8547(97)00122-5.

[53] S. Bockel, J. Amorim, G. Baravian, A. Ricard, and P. Stratil. " A spectroscopic study of active species in DC and HF flowing discharges in-and Ar–mixtures. ". *Plasma Sources Science and Technology.*, **5** (3):567, 1666.
DOI: https://doi.org/10.1088/0963-0252/5/3/026.

[54] S. D. Popa. "Influence of pressure on spectral intensities in a flowing nitrogen glow discharge.". *Journal of Physics D: Applied Physics*, **29**(2):416, 1996.
DOI: https://doi.org/10.1088/0022-3727/29/2/019.

[55] K. Behringer and U. Fantz. "Spectroscopic diagnostics of glow discharge plasmas with non-Maxwellian electron energy distributions.". *Journal of Physics D: Applied Physics*, **27**(10):2128, 1994.
DOI: https://doi.org/10.1088/0022-3727/27/10/021.

[56] D. Wang, D Zhao, K. Feng, X. Zhang, D. Liu, and S. Yang. "The cold and atmospheric-pressure air surface barrier discharge plasma for large-area sterilization applications.". *Applied Physics Letters*, **98**(16), 2011.
DOI: https://doi.org/10.1063/1.3582923.

[57] N. K. Bibinov, A. A. Fateev, and K. Wiesemann. "On the influence of metastable reactions on rotational temperatures indielectric barrier discharges in He-N_2 mixtures.". *Journal of Physics D: Applied Physics*, **34**(12):1819, 2001.
DOI: https://doi.org/10.1088/0022-3727/34/12/309.

[58] V. Milosavljevic and P. J. Cullen. "Spectroscopic investigation of a dielectric barrier discharge in modified atmosphere packaging. ". *The European Physical Journal Applied Physics*, **80**(2):20801, 2017.
DOI: https://doi.org/10.1051/epjap/2017170201.

[59] V. M. Donnelly. "Plasma electron temperatures and electron energy distributions measured by trace rare gases optical emission spectroscopy.". *Journal of Physics D: Applied Physics.*, **37**(19):R217, 2004.
DOI: https://doi.org/10.1088/0022-3727/37/19/R01.

[60] J. B. Boffard, C. C. Lin, and C. A. DeJoseph Jr. "Application of excitation cross sections to optical plasma diagnostics.". *Journal of Physics D: Applied Physics*, **37**(12):R143, 2004.
DOI: https://doi.org/10.1088/0022-3727/37/12/R01.

[61] G. Norlen. "Wavelengths and energy levels of Ar I and Ar II based on New Interferometric Measurements in the Region 3 400-9 800 Å.". *Physica Scripta*, **8**(6):249, 1973.
DOI: https://doi.org/10.1088/0031-8949/8/6/007.

[62] A. Lofthus and P. H. Krupenie. "The spectrum of molecular nitrogen.". *Journal of physical and chemical reference Data*, **6**(1): 113–307, 1977.
DOI: https://doi.org/10.1063/1.555546.

[63] H. R. Griem. "Plasma Spectroscopy ". *McGraw-Hill, New York*, **1**: 386, 1964.

[64] T. G. Owano, M. H. Gordon, and C. H. Kruger. "Measurements of the radiation source strength in argon at temperatures between 5000 and 10 000 K.". *Physics of Fluids B: Plasma Physics*, **2**(12): 3184–90, 1990.
DOI: https://doi.org/10.1063/1.859228.

[65] M. D. Calzada, A. Rodero, A. Sola, and A. Gamero. "Excitation kinetic in an argon plasma column produced by a surface wave at atmospheric pressure.". *Journal of the Physical Society of Japan*, **65** (4):948–54, 1996.
DOI: https://doi.org/10.1143/JPSJ.65.948.

[66] T. Fujimoto and R. W. McWhirter. "Validity criteria for local thermodynamic equilibrium in plasma spectroscopy.". *Physical Review A*, **42**(11):6588, 1990.
DOI: https://doi.org/10.1103/PhysRevA.42.6588.

[67] C. O. Laux, R. J. Gessman, C. H. Kruger, F. Roux, F. Michaud, and S. P. Davis. "Rotational temperature measurements in air and nitrogen plasmas using the first negative system of N^{2+}.". *Journal of Quantitative Spectroscopy and Radiative Transfer.*, **68**(4):473–82, 2001.
DOI: https://doi.org/10.1016/S0022-4073(00)00083-2.

[68] G. Herzberg. " Molecular Spectra and Molecular Structure I: Spectra of Diatomic Molecules". *Van Nostrand, New York*, , 1950.

[69] D. R. Lide. "Handbook of Chemistry and Physics ". *CRC Press, Boca Raton*, , 2001.

[70] "National Institute of Standards and Technology". *NIST: Atomic Spectra Data Base (Gaithersburg, MD: NIST Physics Laboratory)*, , 1979-2008.

[71] D. H. Winicur and J. L. Fraites. "Electronic-energy exchange cross sections for Ar*(3 P) and N 2 (X 1 ∑ g+). ". *The Journal of Chemical Physics*, **61**(4):1548–53, 1974.
DOI: https://doi.org/10.1063/1.1682099.

[72] J. Levaton, J. Amorim, and D. Franco. "Experimental and calculated N (4S) temporal density profile in the N_2 flowing post-discharge. ". *Journal of Physics D: Applied Physics*, **38**(13):2204, 2005.
DOI: https://doi.org/10.1088/0022-3727/38/13/019.

[73] G. G. Raju. "Collision cross sections in gaseous electronics part I: what do they mean.". *IEEE electrical insulation magazine*, **22**(4): 5–23, 2006.
DOI: https://doi.org/10.1109/MEI.2006.1678354.

[74] R. S. Chang and D. W. Setser. "Radiative lifetimes and two-body deactivation rate constants for Ar (3 p 5, 4 p) and Ar (3 p 5, 4 p′) states.". *The Journal of Chemical Physics*, **69**(9):3885–97, 1978.
DOI: https://doi.org/10.1063/1.437126.

[75] M. Qian, C. Ren, D. Wang, J. Zhang, and G. Wei. "Stark broadening measurement of the electron density in an atmospheric pressure argon plasma jet with double-power electrodes. ". *Journal of Applied Physics*, **107**(6), 2010.
DOI: https://doi.org/10.1063/1.3330717.

[76] A. Y. Nikiforov, C. Leys, M. A. Gonzalez, and J. L. Walsh. "Electron density measurement in atmospheric pressure plasma jets: Stark broadening of hydrogenated and non-hydrogenated lines.". *Plasma Sources Science and Technology*, **24**(3):034001, 2015.
DOI: https://doi.org/10.1088/0963-0252/24/3/034001.

[77] J. M. Mermet. "Inductively Coupled Plasma Emission Spectroscopy edited by PWJM Boumans". *Wiley, New York*, , 1987.

[78] C. O. Laux, T. G. Spence, C. H. Kruger, and R. N. Zare. "Optical diagnostics of atmospheric pressure air plasmas.". *Plasma Sources Science and Technology*, **12**(2):125, 2003.
DOI: https://doi.org/10.1088/0963-0252/12/2/301.

[79] S. G. Belostotskiy, T. Ouk, V. M. Donnelly, D. J. Economou, and N. Sadeghi. "Gas temperature and electron density profiles in an argon dc microdischarge measured by optical emission spectroscopy.". *Journal of applied physics*, **107**(5), 2010.
DOI: https://doi.org/10.1063/1.3318498.

[80] F. J. Mehr and M. A. Biondi. "Electron-temperature dependence of electron-ion recombination in Argon.". *Physical Review*, **176**(1):322, 1968.
DOI: https://doi.org/10.1103/PhysRev.176.322.

[81] M. A. Gigosos and V. Cardenoso. "New plasma diagnosis tables of hydrogen Stark broadening including ion dynamics. ". *Journal of Physics B: Atomic, Molecular and Optical Physics*, **29**(20):4795, 1996.
DOI: https://doi.org/10.1088/0953-4075/29/20/029.

[82] D. Staack, B. Farouk, A. Gutsol, and A. Fridman. "Characterization of a dc atmospheric pressure normal glow discharge. ". *Plasma Sources Science and Technology*, **14**(4):700, 2005.
DOI: https://doi.org/10.1088/0963-0252/14/4/009.

[83] N. Haraki, S. Nakano, S. Ono, and S. Teii. "Oxygen radical density measurement in O_2–N_2 gas mixture plasma by means of a thin platinum wire. ". *Electrical Engineering in Japan*, **149**(4):14–20, 2004.
DOI: https://doi.org/10.1002/eej.20018.

[84] J. C. Thomaz, J. Amorim, and C. F. Souza. "Validity of actinometry to measure N and H atom concentration in N_2-H_2 direct current glow discharges. ". *Journal of Physics D: Applied Physics*, **32**(24):3208, 1999.
DOI: https://doi.org/10.1088/0022-3727/32/24/317.

[85] M. A. Lieberman and A. J. Lichtenberg. "Principles of Plasma Discharge and Materials Processing". *Wiley, New York, 1994*, **1**:487.

[86] J. T. Gudmundsson and E. G. Thorsteinsson. "Oxygen discharges diluted with argon: dissociation processes.". *Plasma Sources Science and Technology*, **16**(2):399, 2007.
DOI: https://doi.org/10.1088/0963-0252/16/2/025.